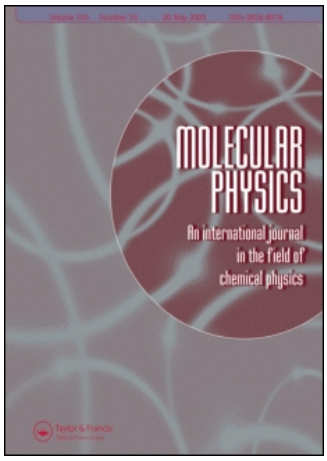

Molecular Physics
An International Journal in the Field of Chemical Physics
Publication details, including instructions for authors and subscription information:
http://www.informaworld.com/smpp/title~content=t713395160

Grand-canonical ensemble Monte Carlo study of dense liquid

Mihaly Mezei [a]
[a] Chemistry Department and Center for Study of Gene Structure and Function, Hunter College of the City University of New York. New York, N.Y.. U.S.A.

Online Publication Date: 20 June 1987
To cite this Article: Mezei, Mihaly , (1987) 'Grand-canonical ensemble Monte Carlo study of dense liquid', Molecular Physics, 61:3, 565 - 582
To link to this article: DOI: 10.1080/00268978700101321
URL: http://dx.doi.org/10.1080/00268978700101321

MOLECULAR PHYSICS, 1987, VOL. 61, NO. 3, 565–582

Grand-canonical ensemble Monte Carlo study of dense liquid Lennard-Jones, soft spheres and water

by MIHALY MEZEI
Chemistry Department and Center for Study of Gene Structure and Function,
Hunter College of the City University of New York,
695 Park Avenue, New York, N.Y. 10021, U.S.A.

(*Received 27 October 1986; accepted 12 January 1987*)

The cavity biased Monte Carlo method for the (T, V, μ) ensemble has been tested on a system of Lennard-Jones particles near the triple point in the liquid and fluid state, on a system of dense soft spheres and on liquid water at room temperature. We demonstrate that the original (T, V, μ) algorithm of Adams is capable to provide accurate density at much higher densities than it was originally thought possible.

1. Introduction and background

The purpose of this work is to study the capabilities of the cavity biased Monte Carlo method (in the following: CB/TVM) [1] for computing configurational averages of dense liquids in the grand-canonical ensemble. Probably the most important advantage of simulations in the grand-canonical ensemble is that they can yield the excess chemical potential directly, making the calculation of the excess free energy possible. Since the computation of the free energy by computer simulation poses particular difficulties, this fact itself may make the additional effort of performing the simulation in the (T, V, μ) ensemble worthwhile. Because of the importance of the free energy, special emphasis will be laid on this aspect of the results.

The CB/TVM method is an extension of the method developed by Adams [2] and independently by Norman and Filinov [3] for Monte Carlo calculations in the grand-canonical ensemble (in the following: TVM). This method is derived from the canonical ensemble Metropolis algorithm [4] by supplementing the stochastic walk generated in the configuration space by random insertions and deletions of a particle. Variations of this method were given by Rowley, Nicholson and Parsonage [5] and by Yao, Greenkorn and Chao [6]. A technique to compute the excess chemical potential in the canonical or microcanonical ensemble was originally suggested by Widom [7] and used in a simulation by Romano and Singer [8]. A variation of this method, called the 'inverse Widom' technique was proposed by Shing and Gubbins [9]. Recently, Powles, Evans and Quirke have observed that the Widom method gives good results even near the triple point of the LJ fluid when implemented in a molecular dynamics simulation [10]. Shing and Gubbins [11] derived and tested an improved version of this method using biased sampling. For the related problem of the computation of the excess free energy, several techniques exist: thermodynamic integration [12], the exponential formula with umbrella sampling (also called the perturbation method) [13], Bennet's method [14, 15] and the recently introduced overlap ratio method of Quirke and Jacucci [16]. Recent reviews of the problem of free-energy calculation can be found in [17–21].

In §2 the CB/TVM method will be reviewed. Computational details can be found in Appendices 1–3. In §3, CB/TVM and TVM calculations are presented for the Lennard-Jones liquid (LJ) near the triple point in the liquid phase and in the fluid phase. By comparing the results of the CB/TVM run with existing data on the LJ fluid, we will establish that the CB/TVM method is able to give reasonably accurate results in this 'difficult' region of the phase space. By comparing the CB/TVM results with the TVM results, we will establish the quantities that we can expect to obtain with reasonable precision at low acceptance rates. In particular, we will demonstrate that the density can be calculated with sufficient accuracy that the excess chemical potential can be determined from it. Section 4 gives the result on the soft sphere system that was used as a reference to determine the excess free energy of the MCY water [22]. Section 5 presents results on the application of the CB/TVM method to water using the ST2 [23], SPC [24] and MCY [25] potentials. Where possible the excess free energy is compared with values recently calculated by thermodynamic integration [22]. Section 6 discusses the results and comments on the relative efficiency of different techniques for free-energy calculation.

2. Theory

Computer simulation in the (T, V, μ) ensemble can be performed by a method that is a direct generalization of the (T, V, N) metropolis Monte Carlo method [2, 3]. A Markov chain of configurations is generated where successive members of the chain are generated from the preceding ones by any of the following three operations: (*a*) displacement of a particle; (*b*) insertion of a particle; (*c*) deletion of a particle. The displacements are accepted using the rules appropriate to the (T, V, N) ensemble. In the present study force-biased displacements [26] were used for the LJ liquid and regular Metropolis displacements [4] for water. The recently introduced CB/TVM method attempts the insertion at positions where a cavity of suitable radius R_c or larger exists and this attempt is accepted with probability.

$$P^i_{CB} = \min\,(1,\, V' P^N_c(\mathbf{r}^N) \exp\,[(\mu + U(\mathbf{r}^N) - U(\mathbf{r}^{N-1}))/kT]/(N+1)). \tag{1}$$

Here μ is the chemical potential, $V' = V\Lambda^3$, where Λ is the de Broglie wavelength, $U(\mathbf{r}^N)$ is the potential energy of a system of N particles at the configuration $\mathbf{r}^N$ and $P^N_c(\mathbf{r}^N)$ is the probability of finding a cavity of radius R_c or larger in the configuration $\mathbf{r}^N$. In Appendix 1 two methods are described that make the cavity search rather efficient for systems of hundreds of particles. Finally, the particle to be deleted is chosen randomly and the deletion attempt is accepted with probability

$$P^d_{CB} = \min\,(1,\, N \exp\,[(-\mu + U(\mathbf{r}^N) - U(\mathbf{r}^{N-1}))/kT]/(V' P^{N-1}_c(\mathbf{r}^{N-1})). \tag{2}$$

The above expressions can be simplified for computational purposes [2] using the substitution

$$\mu' = kTB - kT \ln \langle N \rangle, \tag{3}$$

where μ' is the excess chemical potential and the value of B is fixed at the beginning of the calculation.

It is possible that no cavity is found in a given configuration and in this case a random insertion is performed. This affects the acceptance of the deletion step since it has to reflect the fact that not all insertions are made into cavities. As described in [1], this requires the estimate of the probability of these random insertions, P^N_{nocav}.

For the moderate density used in [1],

$$P^N_{\text{nocav}} = (1 - P^N_c)^{N_t} \tag{4}$$

provided an adequate estimate. However, since in general $\langle(1 - P^N_c)^{N_t}\rangle \neq (1 - \langle P^N_c(\mathbf{r}^N)\rangle)^{N_t}$, for the higher densities used in the present work it is necessary to estimate P^N_{nocav} directly from the simulation. Fortunately, this required only a small extra effort.

There is considerable freedom in choosing the order of the various types of trial perturbations. The present work, follows Adams [2], in performing displacement, insertion, displacement, deletion attempts in cycles.

For particles that lack spherical symmetry (like water) the orientation of the particle has to be chosen at an insertion. In the present work we always chose a random orientation. It is possible, that by considering the torques at the insertion site selected, an efficient orientation selection, analogous to the gradient bias methods [26, 28], can be developed.

2.1. *Density limitations*

It is well known that at high densities the frequency of successful insertion in (T, V, μ) simulations will become negligible since the attempted insertion will always cause an overlap with existing molecules. This limitation motivated the development of the cavity-biased algorithm and one of the goals of the present paper is to explore this limit.

Interestingly, at low densities a different kind of problem can arise. A state that lies inside the coexistence curve is metastable. Therefore, simulations at this point for sufficiently large systems and sufficiently long simulation length should separate into a liquid and a vapour phase. However, for smaller systems the liquid state appears to be artificially stabilized, and this has been observed in a large number of simulations in the (T, V, N) and (E, V, N) ensembles. Simulations in the (T, V, μ) ensemble, however, are less stable at lower densities and the separation occurs rapidly even at small system sizes. An example of this phenomenon will be presented in § 3.3.

2.2. *The estimation of* $P^N_c(\mathbf{r}^N)$

The estimation of $P^N_c(r^N)$ can be performed at several levels of approximation:

(1) $P^N_c(\mathbf{r}^N)$ can be approximated by a configuration independent P^N_c, see [1]. This is simple computationally and was found to be adequate for the supercritical LJ fluid at moderate density. In the present work results will be presented near the triple point of the fluid where it leads to a ~ 1 per cent error in $\langle N\rangle$. Calculations using this method will be labelled CB/TVM/M (the suffix M indicates the use of the mean probabilities).

(2) $P^N_c(\mathbf{r}^N)$ can be approximated by averaging the estimated probability of finding a cavity only over configurations that resulted in a successful insertion or deletion. The label CB/TVM/AM method will refer to this technique (the suffix AM indicates the use of the mean probabilities over accepted insertions and deletions).

(3) The 'exact' procedure estimates $P^N_c(\mathbf{r}^N)$ separately at each configuration $\mathbf{r}^N$. This, however, is only workable if the estimate is precise enough, making it

impractical for the random cavity search involved with either CB/TVM/M or CB/TVM/AM. Its use requires a different approach. Following Owicki and Scheraga [27], we implemented a cavity search using a finite grid. Insertions are performed on a randomly selected 'free' grid. This introduces a slight error into the limiting distribution of the Markov chain since the deletions can occur at any point in the box but the insertions are restricted to the gridpoints. The error decreases as the grid is refined. It will be demonstrated that the error is actually negligible with manageable gridsizes. Details of the algorithm are given in Appendix 3. The method using this grid algorithm will be labelled CB/TVM/GX.

2.3. *Calculation of the free energy*

The excess free energy per particle A' can be obtained from the excess chemical potential and pressure using the expression

$$A' = \mu' - pV/N + kT = kT[B - \ln \langle N \rangle - pV/(NkT) + 1] \tag{5}$$

where p is the pressure of the liquid. It can be computed from the virial sum and a correction term due to the finite cutoff applied to the potential [2, 29, 30]. The configurational free energy per particle A_c is obtained using equation (5) as

$$A_c = A' + kT(\ln \rho - 1) = kTB - pV/\langle N \rangle - kT \ln V. \tag{6}$$

2.4. *Extrapolation to a target density*

(T, V, μ) ensemble calculations provide only the excess chemical potential at a density that is obtained at the end of the calculation as an ensemble average. To obtain results at a preassigned density, it may be necessary to perform additional (T, V, μ) simulations, and then interpolate. However, results from one run close to the density targeted should give a good estimate for the B value necessary to obtain the required $\langle N \rangle$ since $\Delta\langle N \rangle/\Delta\mu$ can be approximated by $(\partial\langle N \rangle/\partial\mu)_{T,V}$ and [2]

$$(\partial\langle N \rangle/\partial\mu)_{T,V} = (\langle N^2 \rangle - \langle N \rangle^2)/kT. \tag{7}$$

Using equation (3) we obtain

$$(\partial\langle N \rangle/\partial B)_{T,V} = (\partial\langle N \rangle/\partial\mu)_{T,N}\, d\mu/dB = \langle N^2 \rangle - \langle N \rangle^2. \tag{8}$$

Similarly, the internal energy and the pressure can be estimated from a run that gives $\langle N \rangle$ close to the requested value

$$(\partial U/\partial\langle N \rangle)_{T,V} = (\partial U/\partial V)_{T,N}\, dV/d\langle N \rangle = (p - \rho kT)/\rho. \tag{9}$$

and

$$(\partial p/\partial\langle N \rangle)_{T,V} = (\partial p/\partial V)_{T,N}\, dV/d\langle N \rangle = kT\rho/(\langle N^2 \rangle - \langle N \rangle^2). \tag{10}$$

Equation (9) can be obtained in an analogous manner to the pressure equation [29] and equation (10) follows from the expression for the isothermal compressibility χ given by Adams [2]

$$\chi = -(\partial V/\partial p)_{T,N}/V = (\langle N^2 \rangle - \langle N \rangle^2)/\rho kT\langle N \rangle. \tag{11}$$

A more general approach can yield the expectation value of any property Q at a chemical potential μ which is different from the one used, μ_0 through a weighted

average over the configurations sampled:

$$\langle Q \rangle_\mu = \langle Q \exp [N(\mu - \mu_0)/kT] \rangle_{\mu_0} / \langle \exp [N(\mu - \mu_0)/kT] \rangle_{\mu_0}. \quad (12)$$

Equation (12) is only limited by the fact that for very different μ and μ_0 the precision of the averages involved would be rather low.

3. Calculations and results on the Lennard-Jones fluid

3.1. *Liquid state near the triple point*

We selected the LJ fluid at $T = 0{\cdot}75$, $\rho = 0{\cdot}8$ for testing the TVM and the different CB/TVM methods at high density. (In describing the LJ results, the usual reduced units are used: $kT/\varepsilon \Rightarrow T$, $V/\sigma^3 \Rightarrow V$, $U/\varepsilon \Rightarrow U$, $p\sigma^3/\varepsilon \Rightarrow p$.) This system is in the liquid state near the triple point of the liquid and is a severe test of the methods. The configurational free energy per particle, A_c, was computed using thermodynamic integration by Hansen and Verlet [31] as $-4{\cdot}27 \pm 0{\cdot}04$ and by Torrie and Valleau [13], using umbrella sampling, $-4{\cdot}265 \pm 0{\cdot}02$. For the pressure, Hansen and Verlet reported $-0{\cdot}319 \pm 0{\cdot}03$ [31] and recently Mezei [32] $-0{\cdot}281$. The system was modelled with a simulation cell of volume $V = 125\,\sigma^3$ with face-centred cubic periodic boundary conditions (FCC PBC) for all but the CB/TVM/GX calculations. With $N = 100$ this corresponds to $\rho = 0{\cdot}8$. The FCC PBC were chosen since about 30 per cent less particles are needed for a given inscribed sphere than for the usual simple cubic boundary conditions. The algorithm and computer code to determine the nearest image of a particle using FCC PBC is due to J. C. Owicki [33]. Appendix 2 provides an algorithm for efficient generation of uniformly distributed random points in an FCC cell, required for the insertion step. For reasons given in Appendix 3, the CB/TVM/GX calculations were performed in a simple cubic cell (SC PBC) with $V = 212{\cdot}5\,\sigma^3$. Here $N = 170$ corresponds to $\rho = 0{\cdot}8$. These system sizes were chosen to obtain an inscribed sphere radius of $\sim 3\,\sigma$. The cavity radius was chosen to be $0{\cdot}8\,\sigma$.

Substituting the previously computed A_c and p values into equation (6) we obtain $B = -1{\cdot}396$ or $B = -1{\cdot}333$ for $N = 100$ when the pressure values of [31] or [32] are used, respectively. For $N = 170$, we obtain $B = -0{\cdot}864$ and $-0{\cdot}801$, respectively.

A spherical cutoff of $2{\cdot}5\,\sigma$ was employed in all simulations and the energy, pressure and entropy for the LJ system were corrected to infinite system size, as described in [29]. Appendix 4 corrects [1] where incorrect long-range correction was used.

Three simulations were performed using $B = -1{\cdot}396$: a run of 3×10^6 steps using Adams' TVM method, a run of 1×10^6 steps using the CB/TVM/M method and a run of 1×10^6 steps using CB/TVM/AM method. In the CB/TVM/M and CB/TVM/AM calculations 200 test points were generated at each insertion step. The corresponding calculations using the CB/TVM/GX method were performed using B $= -0{\cdot}865$ with gridsizes $0{\cdot}3\,\sigma$, $0{\cdot}15\,\sigma$ and $0{\cdot}10\,\sigma$. The acceptance probability of the insertion/deletion step was 0·001 and 0·02 for the TVM and CB/TVM methods, respectively. The $\langle N \rangle$ values obtained were $99{\cdot}8 \pm 0{\cdot}6$, $98{\cdot}7 \pm 0{\cdot}8$ and $99{\cdot}4 \pm 0{\cdot}7$ for the TVM, CB/TVM/M and CB/TVM/AM methods, respectively. (The error bounds were obtained by the method of batch means [34].) The CB/TVM/GX method gave $\langle N \rangle = 166{\cdot}9 \pm 1{\cdot}0$, $169{\cdot}1 \pm 0{\cdot}4$ and $169{\cdot}2 \pm 0{\cdot}6$, for grid-

sizes $0{\cdot}3\sigma$, $0{\cdot}15\sigma$ and $0{\cdot}10\sigma$, respectively. For gridsizes $0{\cdot}15\sigma$ and $0{\cdot}10\sigma$ the calculations were repeated with slightly different setup parameters, giving $\langle N\rangle = 169{\cdot}1 \pm 0{\cdot}5$ and $\langle N\rangle = 168{\cdot}9 \pm 0{\cdot}6$, respectively. The various thermodynamic parameters and run characteristics at successive stages of the runs are collected in tables 1 and 2. The numbers in the tables printed in bold face correspond to the results at the end of a run. The same quantities at intermediate stages of the calculation are also given in these tables to show the convergence characteristics of the various quantities. Part of the data will be discussed in § 6.

Runs of similar length using $B = -1{\cdot}23$ were also performed. For the insertion/deletion step the acceptance probability was 0·001 and 0·02 for the TVM and CB/TVM/M methods, respectively. The TVM and CB/TVM/M methods gave

Table 1. Thermodynamic parameters and run characteristics for the Lennard-Jones system at $T = 0{\cdot}75$ targeting $\rho = 0{\cdot}8$, $N = 100$.

B	$\langle N\rangle$	$-U$	$-p$	$-s'$	c'_v	α	β	γ	$\beta\gamma/\alpha$	ρ'	dN	NMC
						TVM						
−1·396	99·6	5·76	0·317	3·21	2·52	0·91	0·15	2·7	0·46	0·99	15	1000
	99·8	5·77	0·302	3·20	2·52	0·68	0·11	5·3	0·91	0·81	15	2000
	99·6	**5·77**	**0·314**	**3·21**	**2·51**	**0·62**	**0·11**	**6·3**	**1·08**	**0·74**	**17**	**3000**
Eq. state			0·275			0·70	0·13	5·1				
						CB/TVM/M						
−1·396	98·6	5·66	0·433	3·38	2·48	0·78	0·14	5·5	0·96	0·77	16	250
	98·9	5·72	0·408	3·33	2·44	0·68	0·12	6·3	1·09	0·70	18	500
	99·0	5·74	0·375	3·29	2·45	0·70	0·12	6·1	1·05	0·73	22	750
	98·7	**5·73**	**0·380**	**3·29**	**2·46**	**0·72**	**0·13**	**6·0**	**1·04**	**0·73**	**26**	**1000**
Eq. state			0·339			0·74	0·15	5·5				
						CB/TVM/AM						
−1·396	99·7	5·75	0·296	3·17	2·56	0·91	0·15	4·5	0·68	0·91	28	200
	98·7	5·70	0·353	3·21	2·48	0·87	0·15	3·2	0·55	0·93	29	500
	99·5	5·74	0·307	3·17	2·47	0·91	0·15	2·2	0·37	1·01	26	700
	99·4	**5·74**	**0·314**	**3·18**	**2·44**	**0·88**	**0·15**	**3·0**	**0·51**	**0·94**	**28**	**1000**
Eq. state			0·290			0·71	0·15	6·6				
						TVM						
−1·23	101·3	5·84	0·164	3·21	2·53	1·19	0·20	−6·3	−1·04	1·68	20	1000
	101·5	5·86	0·167	3·23	2·57	0·94	0·15	−0·9	−0·16	1·30	21	2000
	101·3	**5·85**	**0·194**	**3·27**	**2·56**	**0·82**	**0·13**	**1·8**	**0·30**	**1·09**	**21**	**3000**
Eq. state			0·139			0·63	0·14	5·5				
						CB/TVM/M						
−1·23	99·9	5·77	0·272	3·30	2·51	0·51	0·09	5·8	1·05	0·77	16	250
	99·5	5·77	0·304	3·37	2·47	0·63	0·11	5·4	0·96	0·78	17	500
	99·7	5·79	0·302	3·39	2·47	0·64	0·11	5·4	0·94	0·78	18	750
	99·8	**5·77**	**0·288**	**3·34**	**2·46**	**0·65**	**0·11**	**5·8**	**0·99**	**0·76**	**18**	**1000**
Eq. state			0·260			0·69	0·13	5·2				

B, the parameter in equation (3); U, p, computed internal energy and external pressure, corrected to infinite potential cutoff; s', c'_v, computed excess entropy and constant volume heat capacity, uncorrected for the potential cutoff; α, β, γ, expansivity, isothermal compressibility and the pressure coefficient, uncorrected for the potential cutoff; ρ', density computed from fluctuations [2]; dN, range of N values sampled in the segment of the run starting from the point the previous line in the table refers to; NMC, number of compound Monte Carlo steps/1000; the data in the lines of Eq. state was obtained from the equation given in [40].

Table 2. Thermodynamic parameters and run characteristics for the Lennard-Jones system at $T = 0{\cdot}75$ targeting $\rho = 0{\cdot}8$ and $N = 170$.

B	$\langle N\rangle$	$-U$	$-p$	$-s'$	c'_v	α	β	γ	$\beta\gamma/\alpha$	ρ'	dN	NMC
					CB/TVM/GX, $g = 0{\cdot}30\,\sigma$							
−0·865	166·7	5·68	0·486	3·43	2·45	0·72	0·13	4·2	0·77	0·84	18	200
	167·0	5·70	0·491	3·45	2·44	1·02	0·19	−0·9	−0·17	1·22	31	500
	166·7	5·69	0·493	3·44	2·44	0·96	0·18	−0·4	−0·07	1·19	23	700
	166·9	**5·69**	**0·483**	**3·43**	**2·42**	**0·84**	**0·16**	**1·6**	**0·31**	**1·03**	**22**	**1000**
Eq. state			0·375			0·76	0·15	4·9				
					CB/TVM/GX, $g = 0{\cdot}15\,\sigma$ (1st)							
−0·865	169·2	5·75	0·358	3·28	2·45	0·47	0·08	8·2	1·42	0·57	18	200
	168·8	5·74	0·394	3·33	2·43	0·62	0·11	5·3	0·93	0·77	26	500
	168·9	5·75	0·377	3·31	2·44	0·62	0·12	3·8	0·69	0·90	22	700
	169·1	5·76	0·361	3·28	2·49	0·62	0·11	4·4	0·79	0·87	22	1000
	169·1	**5·75**	**0·362**	**3·27**	**2·48**	**0·62**	**0·11**	**4·2**	**0·76**	**0·88**	**23**	**1250**
Eq. state			0·284			0·70	0·14	5·2				
					CB/TVM/GX, $g = 0{\cdot}15\,\sigma$ (2nd)							
−0·865	168·9	5·75	0·393	3·34	2·45	0·49	0·09	6·7	1·21	0·67	18	250
	168·8	5·74	0·394	3·33	2·43	0·62	0·11	5·3	0·93	0·77	26	500
	169·1	5·77	0·363	3·30	2·47	0·63	0·11	3·6	0·66	0·92	22	750
	169·1	5·76	0·361	3·28	2·49	0·62	0·11	4·4	0·79	0·87	21	1000
	169·1	5·75	0·362	3·27	2·48	0·62	0·11	4·2	0·76	0·88	23	1250
	169·1	**5·75**	**0·353**	**3·27**	**3·47**	**0·61**	**0·11**	**4·1**	**0·75**	**0·89**	**20**	**1500**
Eq. state			0·284			0·70	0·14	5·2				
					CB/TVM/GX, $g = 0{\cdot}1\,\sigma$ (1st)							
−0·865	168·6	5·75	0·438	3·41	2·45	0·64	0·11	9·1	1·53	0·51	23	200
	169·6	5·77	0·326	3·24	2·44	0·65	0·11	4·3	0·76	0·86	25	500
	169·5	5·75	0·334	3·22	2·45	0·70	0·12	5·2	0·86	0·80	24	1000
	169·2	**5·76**	**0·347**	**3·26**	**2·45**	**0·68**	**0·12**	**5·2**	**0·90**	**0·80**	**20**	**1250**
Eq. state			0·281			0·70	0·14	5·2				
					CB/TVM/GX, $g = 0{\cdot}1\,\sigma$ (2nd)							
−0·865	170·2	5·79	0·287	3·20	2·43	0·63	0·11	6·7	1·12	0·68	20	200
	168·9	5·75	0·379	3·31	2·42	0·71	0·13	2·2	0·39	1·00	22	500
	168·9	5·75	0·389	3·33	2·45	0·75	0·13	2·3	0·42	1·01	22	800
	168·6	5·74	0·402	3·36	2·44	0·73	0·13	2·4	0·43	1·01	22	1000
	168·8	5·75	0·395	3·34	2·45	0·73	0·13	2·3	0·42	1·01	22	1200
	168·9	**5·75**	**0·387**	**3·32**	**2·46**	**0·74**	**0·13**	**2·2**	**0·40**	**1·02**	**25**	**1500**
Eq. state			0·291			0·71	0·14	5·2				

B, the parameter in equation (3); U, p, computed internal energy and external pressure, corrected to infinite potential cutoff; s', c'_v, computed excess entropy and constant volume heat capacity, uncorrected for the potential cutoff; α, β, γ, expansivity, isothermal compressibility and the pressure coefficient, uncorrected for the potential cutoff; ρ', density computed from fluctuation [2]; dN, range of N values sampled in the segment of the run starting from the point the previous line in the table refers to; NMC, number of compound Monte Carlo steps/1000; the data in the line of Eq. state was obtained from the equation given in [40]; g, gridsize for the insertion algorithm.

$\langle N\rangle = 101{\cdot}3 \pm 0{\cdot}8$ and $99{\cdot}7 \pm 0{\cdot}9$, respectively. The various thermodynamic parameters and run characteristics at successive stages of the runs are given in table 1.

For the CB/TVM/M method, the B and p values can be extrapolated for $\rho = 0{\cdot}8$ as $B = -1{\cdot}18$ and $p = -0{\cdot}260$. Significantly, the use of equations (8) and (10) gave the same result. Table 3 contains the B parameter and the pressure extrapolated to

Table 3. LJ simulation results at $T = 0{\cdot}75$ extrapolated to $\rho = 0{\cdot}80$.

	g	B	$\langle N \rangle$	$\langle \rho \rangle$	p	B^x	p^x	A_c
TVM		−1·396	99·6	0·7968	−0·314	−1·37	−0·296	−4·28
CB/TVM/M		−1·396	98·7	0·7896	−0·380	−1·18	−0·260	−4·18
CB/TVM/AM		−1·396	99·4	0·7952	−0·314	−1·33	−0·354	−4·23
CB/TVM/GX (1st)	0·15	−0·865	169·1	0·7958	−0·362	−0·785	−0·314	−4·22
CB/TVM/GX (2nd)	0·15	−0·865	169·1	0·7959	−0·353	−0·784	−0·305	−4·23
CB/TVM/GX (1st)	0·10	−0·865	169·2	0·7962	−0·347	−0·799	−0·308	−4·23
CB/TVM/GX (2nd)	0·10	−0·865	168·9	0·7950	−0·387	−0·781	−0·337	−4·21

The superscript x indicates extrapolation to $\rho = 0{\cdot}80$.

$\rho = 0{\cdot}8$ and the configurational free energy values computed. Based on the successful use of the extrapolation formulae for the CB/TVM/M calculations we employed equations (8) and (10) to obtain these results. The error estimate for A_c is obtained using equation (8) from the error estimate computed for $\langle N \rangle$. The error in A_c should also have a contribution from p, but the two contributions are likely to be correlated and simple addition of the error squares would lead to an overestimate.

The most striking result is that while the acceptance rate of an insertion/deletion step for the TVM method is about 20 times less than for the CB/TVM methods, the density is accurate to within 1 per cent, implying that even at such a low acceptance rate reasonable accuracy can be obtained for the density. This result has been arrived at independently by Quirke [35].

The differences between the calculated configurational free energies and the previously computed values are all within the stated error limits with the CB/TVM/M result giving the largest deviation. The pressure values generally fall between the two previously published values, the exception again is the CB/TVM/M result.

3.2. *Fluid state near the triple point*

The free energy of the LJ fluid at $T = 0{\cdot}903$ and $\rho = 0{\cdot}835$ was computed by Torrie and Valleau [13] as $A_c = -3{\cdot}966 \pm 0{\cdot}02$ and the pressure has been obtained by McDonald and Singer [36] as 1·09. Using a system of 178 particles requires a simple cubic cell of $5{\cdot}9737\,\sigma$ edge, easily accommodating the $2{\cdot}5\,\sigma$ cutoff for the potential. The previously computed free energy and pressure values suggest $B = 2{\cdot}27$. The initial configuration for the (T, V, μ) ensemble simulation was first equilibrated in the (T, V, N) ensemble, giving $U = -5{\cdot}84 \pm 0{\cdot}01$ and $p = 1{\cdot}08 \pm 0{\cdot}07$, in good agreement with the values given by McDonald and Singer. (T, V, μ) ensemble simulations were performed using the TVM, CB/TVM/M ($R_c = 0{\cdot}7\,\sigma$ and $R_c = 0{\cdot}8\,\sigma$) and the CB/TVM/GX ($R_c = 0{\cdot}8\,\sigma$) method with a $0{\cdot}10\,\sigma$ grid. The acceptance probabilities for the insertion/deletion steps was 0·0004 for the TVM method and 0·004 and 0·015 for the CB/TVM/M method using $R_c = 0{\cdot}7\,\sigma$ and $0{\cdot}8\,\sigma$, respectively. The results at the successive stages of the runs are summarized in table 4. For the average number of particles we obtained $\langle N \rangle = 178{\cdot}0 \pm 1{\cdot}5$, $177{\cdot}5 \pm 1{\cdot}1$, $178{\cdot}3 \pm 1{\cdot}7$ and $178{\cdot}8 \pm 0{\cdot}7$ using the TVM, CB/TVM/M, CB/TVM/M and CB/TVM/GX methods, respectively. The pressure was computed as $p = 1{\cdot}02 \pm 0{\cdot}10$, $0{\cdot}97 \pm 0{\cdot}08$, $1{\cdot}03 \pm 0{\cdot}11$ and $1{\cdot}07 \pm 0{\cdot}08$ using the TVM, CB/TVM/M, CB/TVM/M and CB/TVM/GX methods, respectively.

Table 4. Thermodynamic parameters and run characteristics for the Lennard-Jones system at $T = 0{\cdot}903$ targeting $\rho = 0{\cdot}835$ and $N = 178$.

B	$\langle N\rangle$	$-U$	p	$-s'$	c'_v	α	β	γ	$\beta\gamma/\alpha$	ρ'	dN	NMC
						TVM						
2·47	178·0	5·86	1·000	3·45	2·57	0·27	0·046	8·2	1·36	0·63	12	1000
	178·3	5·86	1·043	3·40	2·53	0·42	0·071	3·7	1·41	1·02	17	2000
	178·0	**5·85**	**1·020**	**3·42**	**2·52**	**0·43**	**0·071**	**3·6**	**0·61**	**1·03**	**15**	**3000**
Eq. state			1·060			0·39	0·069	5·7				
						CB/TVM/GX, $R_c = 0{\cdot}8\,\sigma$, $g = 0{\cdot}1\,\sigma$						
2·47	179·0	5·88	1·137	3·30	2·39	0·45	0·074	2·4	0·39	1·09	21	200
	179·4	5·87	1·132	3·30	2·45	0·52	0·087	−0·0	−0·00	1·35	24	500
	178·6	5·86	1·100	3·33	2·53	0·56	0·092	0·2	0·04	1·35	18	700
	178·7	**5·85**	**1·070**	**3·36**	**2·51**	**0·49**	**0·081**	**2·1**	**0·34**	**1·18**	**14**	**1000**
Eq. state			1·118			0·38	0·067	5·7				
						CB/TVM/M, $R_c = 0{\cdot}7\,\sigma$						
2·47	176·1	5·80	0·868	3·56	2·55	0·26	0·049	7·1	1·33	0·69	13	200
	177·0	5·83	0·913	3·54	2·57	0·37	0·064	5·3	0·92	0·88	17	500
	177·5	5·85	0·961	3·50	2·58	0·41	0·067	5·6	0·92	0·86	16	700
	177·5	**5·84**	**0·967**	**3·49**	**2·55**	**0·46**	**0·077**	**3·5**	**0·59**	**1·04**	**19**	**1000**
Eq. state			1·019			0·39	0·070	5·7				
						CB/TVM/M, $R_c = 0{\cdot}8\,\sigma$						
2·47	177·9	5·86	0·962	3·50	2·38	0·49	0·082	2·4	0·41	1·07	22	200
	178·1	5·87	1·037	3·41	2·36	0·39	0·065	4·5	0·74	0·88	19	500
	178·4	5·85	1·040	3·40	2·45	0·39	0·062	5·8	0·93	0·80	16	700
	178·3	**5·86**	**1·035**	**3·41**	**2·45**	**0·36**	**0·058**	**6·4**	**1·03**	**0·74**	**18**	**1000**
Eq. state			1·084			0·39	0·068	5·7				

B, the parameter in equation (3); U, p, computed internal energy and external pressure, corrected to infinite potential cutoff; s', c'_v, computed excess entropy and constant volume heat capacity, uncorrected for the potential cutoff; α, β, γ, expansivity, isothermal compressibility and the pressure coefficient, uncorrected for the potential cutoff; ρ', density computed from fluctuation [2]; dN, range of N values sampled in the segment of the run starting from the point the previousl line in the table refers to; NMC, number of compound Monte Carlo steps/1000; the data in the line of Eq. state was obtained from the equation given in [40]; g, gridsize for the insertion algorithm.

Extrapolation to $\rho = 0{\cdot}835$ gave $p^x = 1{\cdot}02$, 1·00, 1·00 and 1·02 using the TVM, CB/TVM/M, CB/TVM/M and CB/TVM/GX methods, respectively. Substituting into equation (6) yields the configurational free energy as $A_c = -3{\cdot}83$, $-3{\cdot}77$, $-3{\cdot}85$ and $-3{\cdot}89$ using the TVM, CB/TVM/M, CB/TVM/M and CB/TVM/GX methods, respectively.

3.3. *Liquid state at medium density and low temperature*

The free energy of the LJ fluid at $T = 0{\cdot}75$ and $\rho = 0{\cdot}6$ was computed by Torrie and Valleau [13] as $A_c = -3{\cdot}966$ in good agreement with Hansen and Verlet [13] who reported $A_c = -3{\cdot}9$ and $p = -0{\cdot}9234$. Use of a 128 particle system requires a simple cubic cell of $5{\cdot}9752\,\sigma$ edge, easily accommodating the $2{\cdot}5\,\sigma$ cutoff on the potential. The previously computed free energy and pressure values suggest $B = -1{\cdot}916$. A short (T, V, N) ensemble run started from a random configuration provided the initial configuration for the (T, V, μ) ensemble simulation.

The simulation of this system, however, is unstable. Calculations using $B \leqslant -1{\cdot}15$ finish with no particle in the box after only 3×10^6 configurations. Calculations with $B \geqslant -1{\cdot}08$, on the other hand, filled the box with over 200 particles, again within 3×10^6 configurations.

4. Calculations and results on soft spheres

The excess free energies of several water models were obtained previously by thermodynamic integration [22] using the soft-sphere fluid at $\rho(\varepsilon/kT)^{1/4} = 0{\cdot}74$ as a reference state. We performed (T, V, μ) ensemble calculations on this system. [36] gives the excess free energy per particle of this soft-sphere system as $A' = 7{\cdot}035\,kT$ and $pV/NkT = 15{\cdot}395$ [37]. An attempt to use the original TVM method met with complete failure: in 5×10^6 configurations not a single insertion attempt was accepted. Calculations with the CB/TVM/M method using $B = 26{\cdot}19$ and $B = 25{\cdot}5$ were performed using FCC PBC and targeting $\langle N \rangle = 64$. The cavity radius chosen was again $0{\cdot}8\,\sigma$ (the volume was $61{\cdot}16\,\sigma^3$). With $B = 25{\cdot}5$ we also performed a calculation using a cavity radius of $0{\cdot}75\,\sigma$. The results of the CB/TVM/M runs are given in table 5. They gave $\langle N \rangle = 65{\cdot}2 \pm 0{\cdot}3$ and $64{\cdot}1 \pm 0{\cdot}3$, $pV/NkT = 15{\cdot}34 \pm 0{\cdot}3$ and $15{\cdot}39 \pm 0{\cdot}2$, respectively. Extrapolation to $\langle N \rangle = 64$ gives $A' = 6{\cdot}91 \pm 0{\cdot}3\,kT$ and $6{\cdot}96 \pm 0{\cdot}3\,kT$, respectively, in good agreement with the value in [37]. The corresponding CB/TVM/GX calculations targeted $N = 91$, using $B = 26{\cdot}54$ corresponding to the $B = 26{\cdot}19$ calculation, employing $0{\cdot}11\,\sigma$ and $0{\cdot}07\,\sigma$ grids. The results of the CB/TVM/GX calculations are summarized in table 6. They

Table 5. Thermodynamic parameters and run characteristics for the soft sphere system targeting $\rho(\varepsilon/kT)^{1/4} = 0{\cdot}74$ and $N = 64$.

B	$\langle N \rangle$	U	pV/NkT	$-s'$	c'_v	α	β	γ	$\beta\gamma/\alpha$	ρ'	dN	NMC
					CB/TVM/M, $R_c = 0{\cdot}8\,\sigma$							
26·19	63·92	3·58	16·00	4·14	3·14	0·10	0·014	4·5	0·64	0·77	17	250
	65·37	3·79	17·28	3·05	3·04	0·31	0·044	29·3	4·11	2·70	5	500
	65·19	3·76	17·09	3·22	3·02	0·23	0·035	22·6	3·39	2·18	6	750
	65·23	**3·76**	**17·11**	**3·20**	**2·95**	**0·20**	**0·030**	**18·3**	**2·78**	**1·88**	**5**	**1000**
Eq. state			15·07			0·13	0·019	6·7				
					CB/TVM/M, $R_c = 0{\cdot}8\,\sigma$							
25·5	64·09	3·60	15·40	3·36	3·07	0·12	0·018	5·6	1·18	1·04	10	225
	64·09	**3·57**	**15·34**	**3·45**	**2·97**	**0·12**	**0·018**	**7·0**	**1·04**	**1·03**	**8**	**500**
Eq. state			14·46			0·13	0·020	6·4				
					CB/TVM/M, $R_c = 0{\cdot}725\,\sigma$							
25·5	64·05	3·59	15·37	3·40	2·96	0·16	0·021	7·2	0·91	1·05	13	300
	64·06	**3·59**	**15·39**	**3·38**	**2·90**	**0·15**	**0·020**	**7·1**	**0·96**	**1·06**	**7**	**500**
Eq. state			14·15			0·13	0·020	6·4				

B, the parameter in equation (3); U, p, computed internal energy and external pressure, corrected to infinite potential cutoff; s', c'_v, computed excess entropy and constant volume heat capacity, uncorrected for the potential cutoff; α, β, γ, expansivity, isothermal compressibility and the pressure coefficient, uncorrected for the potential cutoff; ρ', density computed from fluctuation [2] ($N = 64$ corresponds to $\rho = 1{\cdot}05$); dN, range of N values sampled in the segment of the run starting from the point the previous line in the table refers to; NMC, number of compound Monte Carlo steps/1000; the data in the line of Eq. state was obtained from the equation given in [40]; g, gridsize for the insertion algorithm.

Table 6. Thermodynamic parameters and run characteristics for the soft sphere system targeting $\rho(\varepsilon/kT)^{1/4} = 0{\cdot}74$ and $N = 91$.

B	$\langle N\rangle$	U	pV/NkT	$-s'$	c'_v	α	β	γ	$\beta\gamma/\alpha$	ρ'	dN	NMC
					CB/TVM/GX, $g = 0{\cdot}11\,\sigma$							
26·54	92·2	3·72	16·82	3·44	2·46	0·09	0·013	1·7	0·26	0·80	7	300
	92·5	**3·76**	**17·05**	**3·22**	**2·80**	**0·08**	**0·012**	**2·3**	**0·35**	**0·75**	**6**	**600**
Eq. state			14·97			0·13	0·019	6·6				
					CB/TVM/GX, $g = 0{\cdot}07\,\sigma$							
26·54	92·8	3·76	17·12	3·21	2·73	0·11	0·017	6·9	1·07	1·11	8	300
	92·5	3·75	17·01	3·27	2·78	0·17	0·025	12·8	1·86	1·54	8	600
	92·5	**3·73**	**17·93**	**3·36**	**2·81**	**0·14**	**0·020**	**8·1**	**1·16**	**1·18**	**7**	**1000**
Eq. state			14·97			0·13	0·019	6·6				

B, the parameter in equation (3); U, p, computed internal energy and external pressure, corrected to infinite potential cutoff; s', c'_v, computed excess entropy and constant volume heat capacity, uncorrected for the potential cutoff; α, β, γ, expansivity, isothermal compressibility and the pressure coefficient, uncorrected for the potential cutoff; ρ', density computed from fluctuation [2] ($N = 91$ corresponds to $\rho = 1{\cdot}05$); dN, range of N values sampled in the segment of the run starting from the point the previous line in the table refers to; NMC, number of compound Monte Carlo steps/1000; the data in the line if eq. state was obtained from the equation given in [40]; g, gridsize for the insertion algorithm.

gave $\langle N\rangle = 92{\cdot}5 \pm 0{\cdot}5$ and $92{\cdot}5 \pm 0{\cdot}5$, respectively, and $pV/nkT = 17{\cdot}05 \pm 0{\cdot}4$ and $16{\cdot}93 \pm 0{\cdot}3$, respectively, in good agreement with the CB/TVM/M run. The probability of successful insertion/deletion was only 0·002–0·003 for all of the runs, comparable to the TVM calculations on the LJ $T = 0{\cdot}75$, $\rho = 0{\cdot}8$ system.

5. Calculations and results on liquid water

CB/TVM simulations were also performed on liquid water at the experimental density at 25°C where the excess free energy has been recently calculated by thermodynamic integration for three different water models [22]. Preliminary calculations using different potentials showed that using the original TVM method no accepted insertions or deletions occurred during 5×10^4 trial runs for the MCY [23] and SPC [24] models and only 30 accepted insertions or deletions for the ST2 [25] water. However, most insertions were quickly deleted again, resulting in the sampling of the narrow N range 95–97. The CB/TVM method was able to produce ~0·001 acceptance probability at liquid water density for the ST2 and the SPC potentials (comparable to the soft sphere calculations) but again there were no accepted insertions or deletions for the MCY potential. The excess free energies of these water models were obtained as −16·57 kJ/mol, −22·59 kJ/mol and −18·45 kJ/mol for the MCY, ST2 and SPC waters, respectively (using FCC PBC with 64 molecules where the inscribed sphere radius is 6·9653 Å). Separate (T, V, N) ensemble calculations for this system size gave the pressure as $p = 545$ atm and $p = -301$ atm, respectively, suggesting $B = -5{\cdot}64$ and $B = -4{\cdot}04$ for the ST2 and SPC waters, respectively.

For the CB/TVM/GX calculations, performed on the ST2 and SPC waters, the corresponding SC PBC requires 91 molecules in a box of side 13·9623 Å. The B values reproducing the earlier calculated excess free energy and pressure values are $B = -5{\cdot}29$ and $B = -3{\cdot}72$ for the ST2 and SPC waters, respectively. For the SPC

Table 7. Cumulative averages of the number of molecules during the water simulations.

Model:	SPC	SPC	SPC	SPC	SPC	ST2	ST2
B:	−4·8	−4·5	−4·3	−4·7	−4·5	−3·8	−3·5
g:	0·12 σ	0·12 σ	0·12 σ	0·8 σ	0·8 σ	0·12 σ	0·12 σ
5×10^5	90·4	88·4	94·4	93·1	92·5	88·8	93·4
10×10^5	**89·2**	90·4	**93·4**	**91·5**	92·6	89·7	92·4
15×10^5		91·3			91·1	89·8	90·9
20×10^5		91·4			91·2	90·6	91·3
25×10^5		**91·2**			**91·6**	90·2	91·4
30×10^5						**90·9**	**91·4**
$\langle N^2\rangle - \langle N\rangle^2$:	1·7	6·0	4·3	5·9	8·5	10·4	8·6

B, the parameter in equation (3); g, gridsize for the insertion algorithm.

waters, calculations were performed using $g = 0{\cdot}24\,\sigma$ ($\sigma = 2{\cdot}8$ Å), $g = 0{\cdot}12\,\sigma$ and $g = 0{\cdot}8\,\sigma$. Using $g = 0{\cdot}24\,\sigma$ and $B = -5{\cdot}1$ kept $\langle N\rangle$ well under 91 and using $B = -4{\cdot}8$ kept $\langle N\rangle$ above 93·0. The $g = 0{\cdot}12\,\sigma$ calculations used $B = -4{\cdot}8$, $B = -4{\cdot}5$ and $B = -4{\cdot}3$, giving $\langle N\rangle = 89{\cdot}2 \pm 1{\cdot}3$, $\langle N\rangle = 91{\cdot}2 \pm 1{\cdot}1$ and $\langle N\rangle = 93{\cdot}8 \pm 0{\cdot}8$, respectively. The calculations with the finest grid $g = 0{\cdot}08\,\sigma$ used $B = -4{\cdot}7$ and $B = -4{\cdot}5$, giving $\langle N\rangle = 89{\cdot}4 \pm 1{\cdot}5$ and $\langle N\rangle = 91{\cdot}6 \pm 1{\cdot}1$, respectively. Successive cumulative averages of $\langle N\rangle$ are given in table 7 for the different runs. The cumulative averages clearly show that the $\langle N\rangle$ values undergo large fluctuations. Successive 5×10^5 averages may actually differ by as much as 4 particles. The B value corresponding to the experimental density is estimated as $B = -4{\cdot}6$, giving $-20{\cdot}63$ kJ/mol for the excess free energy of the SPC water.

For the ST2 water CB/TVM/GX calculations were performed using a $0{\cdot}12\,\sigma$ grid since the SPC results showed no statistically significant difference in the computed $\langle N\rangle$ when the finer grid was used. The cavity radius was chosen as $R_c = 2{\cdot}6$ Å. Using $B = -4{\cdot}6$ and $B = -4{\cdot}2$ the density turned out to be significantly lower than the experimental value. Calculations with $B = -3{\cdot}8$ and $B = -3{\cdot}5$ gave $\langle N\rangle = 90{\cdot}9 \pm 1{\cdot}3$ and $91{\cdot}4 \pm 1{\cdot}2$, respectively. The successive cumulative averages for $\langle N\rangle$ are displayed in table 7. The B value corresponding to the experimental density is estimated as $B = -3{\cdot}6$, giving the excess free energy of the ST2 water as $-19{\cdot}37$ kJ/mol.

6. Discussion

It has been shown that the CB/TVM method is capable of simulating the LJ fluid near the triple point. This is a significant improvement over previous grand-canonical ensemble calculations where the highest density used was $\rho = 0{\cdot}64$ [2], $\rho = 0{\cdot}68$ [38] and $\rho = 0{\cdot}6325$ [6]. Similarly, accurate results have been obtained for the excess free energy of the soft-sphere system at high density (or, equivalently, at low temperature). It has also been demonstrated that the original TVM method, in spite of the very low acceptance rate of insertions or deletions, is still capable of producing reasonably accurate results for the LJ systems studied but failed for the dense soft spheres and for liquid water. It has also been demonstrated that simulations in the (T, V, μ) ensemble produce phase separations more easily than in the (T, V, N) or (E, V, N) ensembles.

For the dense atomic fluids, the precision of the calculated $\langle N \rangle$ values with runs of 1×10^6–2×10^6 steps is about 0·5–1 per cent. This gives an estimated error of the order of 0·1 kT in the free energy. This is somewhat larger than the ~0·03–0·05 kT quoted in the literature for the LJ fluid when thermodynamic integration or the perturbation method with umbrella sampling is used. The calculated statistical uncertainties for $\langle N \rangle$ in the liquid water simulations are 1–2 per cent. Here the convergence characteristics are markedly worse than for the model liquids, making the free energy results less reliable. The likely reason for this is the heavy dependence of the deletion probability on the high energy wing of the binding energy distribution: Monte Carlo runs on water show long range energy correlations [26, 39] and the effects are most pronounced at the extremes of the energy distributions.

The ranges of N sampled (shown in the tables as dN) show no significant difference between different segments of a run and were essentially the same for TVM as for CB/TVM for the LJ systems simulated, consistently well over 10 per cent. For the SS system studied, however, dN was generally below 10 per cent and showed larger fluctuations over the various segments of the run. This confirms the earlier finding that this SS system is more difficult to simulate in the (T, V, μ) ensemble than the LJ systems tried.

The excess entropy s' and excess constant volume heat capacity c'_v were computed using expressions given by Adams [2]. The heat capacity shows consistently good convergence behaviour, which is better than the convergence for the entropy. This is surprising, since earlier work on liquid water (albeit in the (T, V, N) ensemble) found its convergence rather poor [26, 39].

The program also computed the fluctuation-dependent thermodynamic properties: the expansivity (α), isothermal compressibility (β) and the pressure coefficient (γ) using the expressions given by Adams [2] that are related to each other by the simple relation $\beta\gamma/\alpha = 1$. For the LJ fluid, the accurate equation of state of Nicolas *et al.* [40] was used to estimate α, β and γ. The values computed from the simulation and estimates from the equation of state are also shown in tables 1, 2 and 4. While the $\beta\gamma/\alpha = 1$ relation is usually strongly violated, the computed α and β values are generally close to the values from the equation of state. Furthermore, they vary monotonously with the density, except for the CBV/TVM/AM calculation. This gives some grounds for considering them to be reasonably accurate. On the other hand, the calculated γ values show no such trend and the value calculated at various stages of a given simulation often varies by factors of two. This is not surprising, since γ is the only fluctuation property that depends on cross-fluctuation. For the soft sphere fluid, the equation of state given by Hoover *et al.* [37] was used to estimate α, β and γ. Here the accuracy of all three of them is markedly worse than for the LJ systems studied. Again, γ is the least reliable. As an additional assessment on the precision of the results an alternative expression for the density, expressed in terms of fluctuations (equation (9) of [2]), has also been evaluated and shown in the tables. The conclusions are in agreement with the conclusions from the $\beta\gamma/\alpha$ check.

Comparison of the different approximations for $P_c^N(\mathbf{r}^N)$ shows that (1) the CB/TVM/M method gives ~1 per cent error in the density; (2) the density obtained by the CB/TVM/AM method appears to be essentially correct but the fluctuation properties are less accurate. The calculations with the CB/TVM/GX method give progressively better results as the cavity-search grid is refined. In particular, the 0·15 σ and 0·10 σ grids both gave essentially the correct density.

The B and p values that were extrapolated to $\rho = 0{\cdot}8$ for the LJ fluid were

obtained using the extrapolation formulae equations (8, 10). The same results are obtained if linear extrapolation is used based on the two CB/TVM/M runs using different Bs. Thus the extrapolation formulae can be used for changes involving $\sim 0{\cdot}5$ per cent in the density.

The failure of the CB/TVM method to produce any density fluctuation with the MCY potential is most likely a consequence of the high pressure of this water model (6000 atm [30]) at the experimental density. For the ST2 and SPC waters, the CB/TVM/GX method produced stable densities with about 5 per cent fluctuation. The computed $\langle N^2\rangle - \langle N\rangle^2$, also shown in table 7, range from 1·7 to 10·4, with the smaller values belonging to the shorter runs. Due to the relatively large error bounds equation (8) is of little use for consistency checks. The computed excess free energies, however, differed from the earlier values from thermodynamic integration by 2·2 kJ/mol and 4·2 kJ/mol, for the SPC and ST2 waters, respectively. Errors of this magnitude cannot be attributed to statistical uncertainties. To make matters worse, the deviations are in the opposite direction, giving a 6·4 kJ/mol discrepancy with the excess free energy difference between the two models previously computed directly by thermodynamic integration [21]. The source of this discrepancy is the subject of further investigations. It probably lies in the difference in the two statistical ensembles since the system sizes applied are rather small.

The computer time requirements on the LJ system of the various techniques can be summarized as follows. Taking the regular canonical ensemble simulation time as one unit, the original TVM technique takes 1·5 units, the CB/TVM/M or CB/TVM/AM methods with $N_t = 200$ take 4·1 units and the CB/TVM/GX technique takes 2·0 and 3·2 units for using 40^3 ($g = 0{\cdot}15\,\sigma$) and 60^3 ($g = 0{\cdot}1\,\sigma$) gridpoints, respectively. However, the memory requirement of the CB/TVM/GX method is 1·5 and 2·7 times the other methods using 40^3 and 60^3 gridpoints, respectively. The overhead involved in the various CB/TVM techniques are about 50 per cent less for the water calculations since this overhead is independent of the potential used.

The comparison of the TVM and CB/TVM methods again demonstrated that the CB/TVM method produces ~ 10 times greater acceptance probabilities for the insertion/deletion step than the TVM method. However, for the LJ systems this difference did not significantly affect the accuracy of the computed configurational averages. On the other hand, for the simulation of the dense soft spheres and liquid water the TVM method was shown to fail while the CB/TVM method produced stable results.

Finally, two novel applications of the (T, V, μ) ensemble simulations are suggested:

(1) The initial configuration for simulation in any ensemble can be generated from scratch very efficiently in the (T, V, μ) ensemble. In our experience, the filling of an empty simulation box and obtaining a reasonably equilibrated configuration is 2–3 times faster in the (T, V, μ) ensemble than the equilibration of a completely random configuration in the (T, V, N) ensemble.

(2) The removal and subsequent insertion of a particle can be considered as a very large step in a canonical ensemble simulation. This can be of significance when the system consists of disjoint or narrowly connected areas where exchange of particles would be nonexistent or extremely rare. Such situation can arise in the simulation of crystal hydrates.

This research was supported by NIH grant 5-R01-GM 24914 and by NSF grant CHE-8203501. Thanks are due to Professor David L. Beveridge for several useful discussions during the course of this project. One of the referees of a very early version is also thanked for helpful criticism.

Appendix 1

Computational details of the cavity search used in the CB/TVM/M and CB/TVM/AM calculations

For large systems, consisting of several hundred particles, some form of neighbour list is essential for an efficient cavity search. For the relatively small systems that we worked with, we found that direct calculation with all particles is possible. There are two simple tricks, however, that are essential in achieving the current speed.

First, the need to find nearest images, any time the distance of a particle from a test point is computed, is eliminated by generating the test points in a reduced cell whose walls are R_c away from the simulation cell's walls. In order to sample all areas of the cell during the simulation, for every insertion attempt the centre of the simulation cell is first translated to a randomly selected point in the simulation cell.

Second, as the distance square between the test point and the particles is computed, an immediate check is made to see if the partial sum exceeds R_c^2 or not. While in some instances the algorithm performs several tests instead of just one, the gain in leaving the loop at an early point far outweighs this disadvantage. In fact, implementation of this second trick made the program run nearly twice as fast for the 100 LJ particles with 200 random points generated for each insertion. For larger systems (or higher dimensions) this gain is even larger.

Appendix 2

Generating uniformly distributed points in an FCC cell

The CB/TVM/M and CB/TVM/AM algorithms require the generation of a large number of points uniformly distributed in the simulation cell. Calculation described here used the FCC lattice because the image to image distance is the largest with a fixed number of particles. A simple procedure would generate random points in a cube containing the simulation cell and then examine if the point is also in the simulation cell itself. This results on the average four boundary condition examinations per random points. To avoid this extra work, we developed here a simple procedure that generates the points directly.

The view of the unit cell from the x-y bisector is shown in figure A 1. Here the plane of the rhombus ABCD is parallel to the plane of the hexagon EFGHIJ. The distance between the two planes is $1/\sqrt{2}$.

The algorithm first selects a plane parallel to these two and lying between them. In general, this carves out a hexagon from the cell labelled in the figure by KLMNOP. The probability of selecting a plane should be proportional to the area of the hexagon carved out, $2r + 2/\sqrt{r}$, where r is the distance of the selected plane from the plane of the rhombus ABCD.

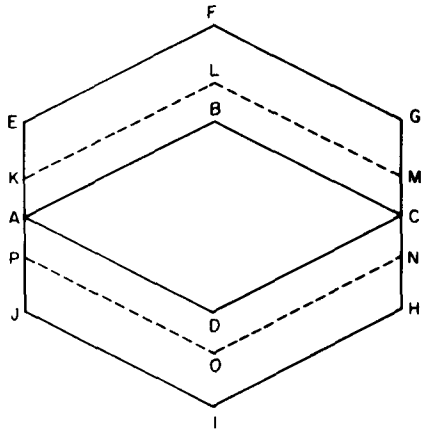

Figure A 1. The unit cell of the FCC PBC viewed from the bisector of the x-y coordinate axes.

Next, a random point is selected in the hexagon KLMNOP. Figure A 2 shows this hexagon with its dimensions as a function of r. A random point will be selected if one first selects a random point in the rectangle KMQR. If the point falls below the ON line, it is translated by $(-1/\sqrt{2},\ 1/2 + r\sqrt{2})$ into the triangle KLS and if the point falls below the OP line, it is translated by $(1/\sqrt{2},\ 1/2 + r\sqrt{2})$ into the triangle LMS.

In the last step, the point is replaced by its mirror image with respect to the plane of the hexagon EFGHIJ with a probability of 0·5. Finally, the coordinates just obtained have to be scaled with the actual size of the cell. Also, in the present implementation the point is rotated by 45 per cent around the z axis since the FCC PBC image search routine of Owicki uses a coordinate system where the coordinate axes go through the vertices of the simulation cell. Implementation of this algorithm gave a $\sim$20 per cent improvement in the overall simulation time over the trivial algorithm for the LJ system using 100 particles and generating 200 random points per insertion.

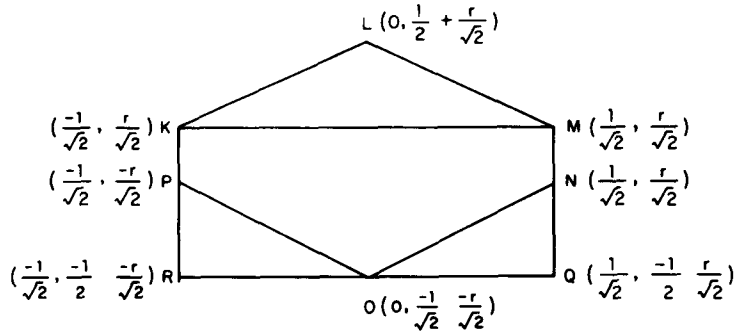

Figure A 2. The unit cell of the FCC PBC cut by a plane perpendicular to the bisector of the x–y coordinate axes.

Appendix 3

The cavity search using the grid algorithm

The algorithm was developed assuming simple cubic periodic boundary conditions. At the outset, an array $N_{cov}(I, J, K)$ is initialized to count the number of particles that are closer than R_c to the grid point $(E0 + I^*EN_g,\ E0 + J^*E/N_g,\ E0 + K^*E/N_g)$, where E is the edge of the simulation cube, $E0 = -E/2 - E/(2^*N_g)$ and N_g is the number of grid points along each axis. At each step, $P_c^N(\mathbf{r}^N)$ is approximated by N_{cav}/N_g^3. The gridsize discussed earlier is E/N_g. Grid points that are not covered are considered to be cavities. A second array L_{cav} contains a list of the cavities, in the form $I^*2^{10} + J^*2^5 + K$. The length of the list L_{cav}, N_{cav} varies during the simulation. Finally, the location of a cavity (I, J, K) is stored in the array N_{cov} (with negative sign to distinguish it from the cover counter values).

When a particle is removed:

(1) For all gridpoints covered by this particle, decrement $N_{cov}(I, J, K)$.

(2) If the decremented $N_{cov}(I, J, K)$ became zero, add (I, J, K) to the cavity list L_{cav} and increment N_{cav}.

When a particle is added:

(1) For each gridpoint covered by this particle that was already covered, increment $N_{cov}(I, J, K)$.

(2) For each cavity covered by this particle, set $N_{cov}(I, J, K)$ to one and remove (I, J, K) from the cavity list. This consists of the following steps:
   2.1. Transfer the information stored in the N_{cav}-th element of the list to the place of the cavity to be removed (obtained from the $N_{cov}(I, J, K)$ corresponding to the cavity);
   2.2. Update the information in the $N_{cov}(I, J, K)$ corresponding to the cavity transferred;
   2.3. Decrement N_{cav}.

A simple displacement can be represented by a removal and an addition although for finer grids it is a rather wasteful procedure.

The main advantage of this algorithm is that the addition or removal of a particle only affects the gridpoints covered by the particle thus the computer time is independent of the system size. The main problem is that the storage requirement increases strongly as the grid is refined.

The restriction of the algorithm to simple cubic cells was necessary to be able to find the cavities covered by a particle without examining the boundary conditions for each gridpoint under study.

Appendix 4

A correction to [1]

All calculations reported in [1] used a correction term to the energy that was double the correct value. As a result, for the system where comparison was made with results of Adams [2] ($T = 2{\cdot}0$, $\rho = 0{\cdot}6408$, $\langle N \rangle = 160{\cdot}2$), a small but noticeable discrepancy was found in the calculated $\langle N \rangle$ that was erroneously attributed to possible problems with the random number generator used in 2. Repeating the calculation (1×10^6 steps) for this system with the correct correction term, we obtained $\langle N \rangle = 160{\cdot}0$ to be compared with 160·2, obtained by Adams. Similar agreements were found for all the properties given in [2].

Note added in proof.—Ruff, Baranyai, Palinkas and Heinzinger published a new version of the CB/TVM/M method where the cavity search is based on the vertices of the Dirichlet–Voronoi polyhedra of the particles and the cavity correction in the acceptance probability is replaced by an energy criterion [41].

References

[1] Mezei, M., 1980, *Molec. Phys.*, **40**, 901.
[2] Adams, D. J., 1975, *Molec. Phys.*, **29**, 311.
[3] Norman, G. E., and Filinov, V. S., 1969, *High Temp. U.S.S.R.*, **7**, 216.
[4] Metropolis, N. A., Rosenbluth, A. W., Rosenbluth, M. N., Teller, A. H., and Teller, E., 1953, *J. chem. Phys.*, **21**, 1087.
[5] Rowley, L. A., Nicholson, D., and Parsonage, P. G., 1975, *J. comput. Phys.*, **47**, 401.
[6] Yao, J., Greenkorn, R. A., and Chao, K. C., 1982, *Molec. Phys.*, **46**, 587.
[7] Widom, B., 1963, *J. chem. Phys.*, **39**, 2808.
[8] Romano, S., and Singer, K., 1979, *Molec. Phys.*, **37**, 1765.
[9] Shing, K. S., and Gubbins, K. E., 1982, *Molec. Phys.*, **46**, 1109.
[10] Powles, J. G., Evans, W. A. B., and Quirke, N., 1982, *Molec. Phys.*, **46**, 1347.
[11] Shing, K. S., and Gubbins, K. E., 1981, *Molec. Phys.*, **43**, 717.
[12] Kirkwood, J. G., 1968, *Theory of Liquids*, edited by B. J. Alder (Gordon & Breach).
[13] Torrie, G., and Valleau, J. P., 1977, *J. comput. Phys.*, **23**, 187.
[14] Bennett, C. H., 1976, *J. comput. Phys.*, **22**, 245.
[15] Jacucci, G., and Quirke, N., 1980, *Molec. Phys.*, **40**, 1005.
[16] Quirke, N., 1980, *Proceedings of the Nato Summer School on Superionic Conductors*, Oderse, Denmark.
[17] Voter, A. F., 1985, *J. chem. Phys.*, **82**, 1890.
[18] Shing, K. S., and Gubbins, K., 1983, *Advances in Chemistry Series*, edited by J. M. Haile and G. A. Mansoori (American Chemical Society).
[19] Levesque, D., Weiss, J. J., and Hansen, J. P., 1984, *Monte Carlo Methods in Statistical Physics* II, edited by K. Binder (Springer-Verlag).
[20] Pratt, L., and Pohorille, A., 1986, *Methods in Enzymology*, Vol. 127, edited by L. Packer (Academic Press).
[21] Mezei, M., and Beveridge, D. L., 1987, *Ann. N.Y. Acad. Sci.*, **482**, 1.
[22] Mezei, M., 1982, *Molec. Phys.*, **47**, 1307.
[23] Matsuoka, O., Clementi, E., and Yoshimine, M., 1976, *J. chem. Phys.*, **64**, 1351.
[24] Stillinger, F. H., and Rahman, A., 1974, *J. chem. Phys.*, **60**, 1545.
[25] Berendsen, H. J. C., Postma, J. P. M., van Gunsteren, W. F., and Hermans, J., 1981, *Intermolecular Forces*, edited by B. Pullman (Reidel).
[26] Pangali, C. S., Rao, M., and Berne, B. J., 1979, *Chem. Phys. Lett.*, **55**, 413. Rao, M., Pangali, C. S., and Berne, B. J., 1979, *Molec. Phys.*, **37**, 1779.
[27] Owicki, J. C., and Scheraga, H. A., 1978, *J. phys. Chem.*, **82**, 1257.
[28] Rossky, P. J., Doll, J. D., and Friedman, H. L., 1978, *J. chem. Phys.*, **69**, 4628.
[29] Barker, J. A., and Henderson, D., 1976, *Rev. mod. Phys.*, **48**, 587.
[30] Mezei, M., and Beveridge, D. L., 1982, *J. chem. Phys.*, **76**, 593.
[31] Hansen, J. P., and Verlet, L., 1969, *Phys. Rev.*, **184**, 151.
[32] Mezei, M., 1983, *Molec. Phys.*, **48**, 1075.
[33] Owicki, J. C. (private communication).
[34] Blackman, R. B., and Tuckey, J. W., 1958, *The Measurement of Power Spectra* (Dover). Wood, W. W., 1968, *Physics of Simple Liquids*, edited by H. N. V. Temperley, J. S. Rowlinson and G. S. Rushbrooke (North-Holland).
[35] Quirke, N. (private communication).
[36] McDonald, I. R., and Singer, K., 1972, *Molec. Phys.*, **23**, 29.
[37] Hoover, W. G., Ross, M., Johnson, K. W., Henderson, D., Barker, J. A., and Brown, B. C., 1970, *J. chem. Phys.*, **52**, 4931.
[38] Adams, D. J., 1976, *Molec.* Phys., **32**, 647.
[39] Mezei, M., Swaminathan, S., and Beveridge, D. L., 1979, *J. chem. Phys.*, **71**, 3366.
[40] Nicolas, J. J., Gubbins, K. E., Streett, W. B., and Tildesley, D. J., 1979, *Molec. Phys.*, **37**, 1429.
[41] Ruff, I., Baranyai, A., Palinkas, G., and Heinzinger, K., 1986, *J. chem. Phys.*, **85**, 2169.